HETE-2 Localization and Observations of the Gamma-Ray Burst GRB 020813

Rie Sato,[1] Takanori Sakamoto,[2] Jun Kataoka,[1] Atsumasa Yoshida,[4,3]
Motoko Suzuki,[3,1] Junichi Kotoku,[1] Yuji Urata,[1,3] Yoshihisa Yamamoto,[1]
Makoto Arimoto,[1] Toru Tamagawa,[3] Yuji Shirasaki,[5] Ken'ichi Torii,[6]
Masaru Matsuoka,[7] Yujin Nakagawa,[4] Toru Yamazaki,[4] Kaoru Tanaka,[4]
Miki Maetou,[4] Makoto Yamauchi,[8] Kunio Takagishi,[8] Donald Q. Lamb,[9]
Jean-Luc Atteia,[10] Roland Vanderspek,[11] Carlo Graziani,[9] Gregory Prigozhin,[11]
Joel Villasenor,[11] J. Garrett Jernigan,[12] Geoffrey B. Crew,[11] Kevin Hurley,[12]
George R. Ricker,[11] Stanford E. Woosley,[13] Nat Butler,[11] Al Levine,[11]
John P. Doty,[11] Timothy Q. Donaghy,[9] Edward E. Fenimore,[14]
Mark Galassi,[14] Michel Boer,[10] Jean-Pascal Dezalay,[15] Jean-Francios Olive,[15]
Joao Braga,[16] Ravi Manchanda,[17] Graziella Pizzichini,[18] and Nobuyuki Kawai[1,3]

[1]*Department of Physics, Tokyo Institute of Technology, Meguro-ku, Tokyo 152-8551*
rsato@hp.phys.titech.ac.jp

[2]*NASA, Goddard Space Flight Center, Greenbelt, MD 20771 USA*

[3]*RIKEN, Hirosawa, Wako, Saitama 351-0198*

[4]*Department of Physics, Aoyama Gakuin University, Sagamihara, Kanagawa 229-8558*

[5]*National Astronomical Observatory of Japan, Osawa, Mitaka, Tokyo 181-8588*

[6]*Department of Earth and Space Science, Graduate School of Science, Osaka University, Toyonaka, Osaka 560-0043*

[7]*JAXA, Sengen, Tsukuba, Ibaraki 304-8505*

[8]*Faculty of Engineering, Miyazaki University, Gakuen Kibanadai Nishi, Miyazaki, Miyazaki 899-2192*

[9]*Department of Astronomy and Astrophysics, University of Chicago, Chicago, IL 60637, USA*

[10]*Laboratoire d'Astrophysique, Observatoire Midi-Pyrénées, 14 Ave. Edouard Belin, 31400 Toulouse, France*

[11]*MIT/CSR 77 Massachusetts Avenue, Cambridge, MA 02139, USA*

[12]*Space Sciences Laboratory, University of California, Berkeley, CA 94720-7450, USA*

[13]*Department of Astronomy and Astrophysics, University of California at Santa Cruz, 477 Clark Kerr Hall, Santa Cruz, CA 95064, USA*

[14]*Los Alamos National Laboratory, P. O. Box 1663 Los Alamos, NM 87545, USA*

[15]*Centre d'Etude Spatiale des Rayonnements, Observatoire Midi-Pyrénées, 9 Avenue du Colonel Roche, 31028 Toulouse, France*

[16]*Instituto Nacional de Pesquisas Espaciais, Avenida Dos Astronautas 1758, São José dos Campos 12227-010, Brazil*

[17]*Department of Astronomy and Astrophysics, Tata Institute of Fundamental Research, Homi Bhabha Road, Mumbai, 400-005, India*

[18]*INAF/IASF Sezione di Bologna, via Piero Gobetti 101, 40129 Bologna, Italy*

(Received 2005 May 20; accepted 2005 September 29)

Abstract

A bright, long gamma-ray burst (GRB) was detected and localized by the instruments on board the High Energy Transient Explorer 2 satellite (HETE-2) at 02:44:19.17 UTC (9859.17 s UT) on 2002 August 13. The location was reported to the GRB Coordinates Network (GCN) about 4 min after the burst. In the prompt emission, the burst had a duration of approximately 125 s, and more than four peaks. We analyzed the time-resolved 2−400 keV energy spectra of the prompt emission of GRB 020813 using the Wide Field X-Ray Monitor (WXM) and the French Gamma Telescope (FREGATE) in detail. We found that the early part of the burst (17−52 s after the burst trigger) shows a depletion of low-energy photons below about 50 keV. It is difficult to explain the depletion with by either synchrotron self-absorption or Comptonization. One possibility is that the low-energy depletion may be understood as a mixture of "jitter" radiation the usual synchrotron radiation component.

Key words: gamma-rays: bursts

1. Introduction

It has been widely accepted that gamma-ray burst (GRB) emission is produced in a shocked optically thin plasma via the synchrotron process (synchrotron shock model; SSM). The resultant emission spectra is a convolution of synchrotron emission from electrons with distributed energies, and can be described as a broken power-law function with a broad νF_ν peak. While the overall spectral shape, particularly at energies around the peak of the spectral energy density and above, depends critically on the energy spectrum of the source electrons, the shape of the low-energy spectrum is bound to converge to a power-law function, $dN/dE \propto E^{-\alpha}$, with index $\alpha = -0.67$, regardless of the source electron spectrum. This is because each of the individual source electron produces emission with the same low-energy asymptotic spectral form, namely a power-law function with an index of $\alpha = -0.67$.

Most of the observed spectra of GRBs are known to be well described by the "Band function" (Band et al. 1993), which is essentially an empirical functional form consisting of two smoothly connected power-law continua, where the spectral index is more negative at higher energies (Preece et al. 2000). The Band function has three parameters to characterize the spectral shape: the low-energy photon spectral index, α, the high-energy photon spectral index, β, and the break energy, E_0. Here, we use the convention that indices α and β are positive in the power-law function, $dN/dE \propto E^{\alpha}$, following Preece et al. (1998). If a photon spectrum produced by the optically thin synchrotron shock is fitted to the Band function, the low-energy photon spectral index, α, cannot be larger than -0.67, because at any part of the

SSM spectrum the photon slope is more negative than -0.67 (e.g., Tavani 1996).

Preece et al. (1998) examined the time-resolved energy spectra of over 100 bright GRBs observed by the BATSE experiment on CGRO, and found 23 bursts in which the spectral index limit of the SSM was violated. Since the spectral measurement of GRBs at energies below 30 keV was difficult for BATSE, Preece et al. (1998) used the "effective spectral index" at 25 keV, i.e. the slope of the power-law tangent to the Band function at the chosen energy (25 keV). Furthermore, Frontera et al. (2000) found several GRBs showing a similar low-energy depletion in the range 2–20 keV, especially during the initial part of the GRB by the BeppoSAX.

In this paper we present the spectral observation of GRB 020813 with the HETE-2 satellite. The FREGATE and WXM detectors on HETE-2 cover a wide energy range of 2–400 keV, and are well suited to study the spectral shape in the X-ray regions. GRB 020813 has one of the highest spectral peak energies, $E_{\rm peak}$, among the GRBs localized by HETE-2 (Sakamoto et al. 2005). We found that part of its time-resolved spectra exhibits a flat low-energy slope that violates the "death line" of the SSM. With its long duration, high fluences and characteristic spectra, GRB 020813 presents an ideal case to study the low-energy part of a hard GRB. Because of its unusual hardness (see figure 4), it is also interesting to study the spectral shape at high energies. That aspect will be presented in a separate paper using the data from another spacecraft, which covers energy ranges higher than those available with HETE-2. In section 2, the properties of GRB 020813 observed by HETE-2 are presented, including a detailed analysis of the time-resolved spectra. In section 3, we discuss the possible process that causes the violation of the SSM limit on the low-energy power-law index. In particular, synchrotron self-absorption and Compton-scattering processes are critically examined.

2. Observation

2.1. Localization

The trigger for this event came from the FREGATE instrument, at 02:44:19.17 UTC (9859.17 s UT) on 2000 August 13. The trigger occurred in the 30−400 keV band, on the 1.3 s time scale. The WXM flight software localized the burst, and its position was RA = $19^{\rm h}46^{\rm m}31^{\rm s}$, Dec = $-19°36'27''$ (J2000.0)[1], with a 90% error radius of $14'$ which includes statistical and systematic errors. The flight location was reported in a GRB Coordinate Network (GCN) Position Notice at 10:50:48 UT, 4 minutes 14 s after the burst. Ground analysis of the WXM data for the burst produced a refined location, which was reported in a GCN Position Notice 117 min after the burst. The WXM location can be expressed as a 90% confidence circle that is $4'$ in radius and is centered at RA = $19^{\rm h}46^{\rm m}41^{\rm s}$, Dec = $-19°38'42''$. Ground analysis of the SXC data for the burst also produced a refined location, which was reported in a GCN Position Notice 184 min after the burst. The SXC location can be expressed as a 90% confidence circle

[1] Hereinafter, equatorial coordinates are J2000.0.

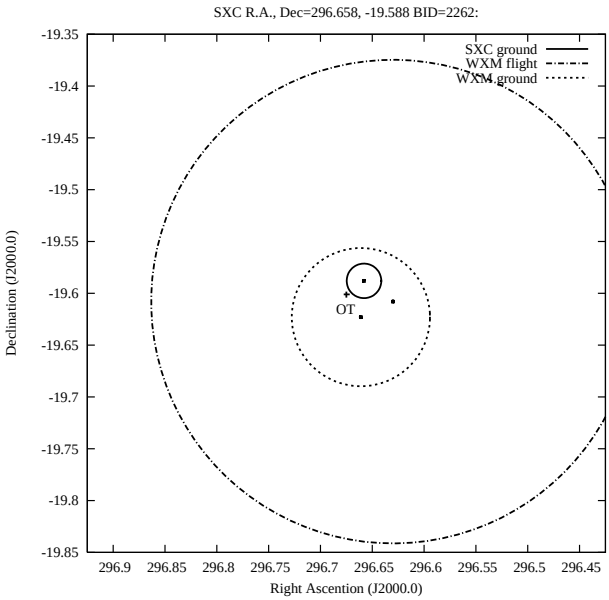

Fig. 1. Sky map summarizing the localization reported in the GCN burst position notices. The error circles represent 90% confidence limits.

that is $60''$ in radius and is centered at RA = $19^{\rm h}46^{\rm m}38^{\rm s}$, Dec = $-19°35'16''$. GRB 020813 was also observed by Interplanetary Network (Ulysses, Konus-Wind, and Mars Odyssey) and the resulting IPN localization was fully consistent with the WXM error circle (Hurley et al. 2002a, 2002b).

An optical afterglow (OT) was observed 112 min after the burst at RA = $19^{\rm h}46^{\rm m}41^{\rm s}.88$, Dec = $-19°36'05''.1$ (Fox et al. 2002) inside the WXM error circle, and follow-up observations were carried out by dozens of telescopes distributed around the world. The light curve of the optical afterglow has shown a break at 14 hr after the burst (e.g., Urata et al. 2003). In the framework of jetted fireballs, this break corresponds to a jet half-opening angle of $1°.9 \pm 0°.2$ (Covino et al. 2003). Moreover, optical spectroscopic observations at the Keck observatory have determined its redshift as $z = 1.255$ (Barth et al. 2003). Figure 1 shows the WXM and SXC localizations, which are consistent with the location of the OT.

2.2. Temporal Properties

Figure 2 shows the complex light curve of GRB 020813 in the four WXM energy bands (2−5, 5−10, 10−17, and 17−25 keV) and the three FREGATE energy bands (6−40, 40−80, and 32−400 keV). There are more than three peaks in the WXM light curve and at least four spiky peaks in the FREGATE light curve. The photon counts in the peaks are higher at later phases. An inspection of the burst light curve in the WXM and FREGATE energy bands shows that the fourth peak is much harder than the others.

Table 1 gives t_{50} and t_{90} durations of GRB 020813 in the 2−5, 5−10, 10−25, and 2−25 keV WXM bands and the 6−40, 40−80, 32−400, and 6−400 keV FREGATE energy bands.

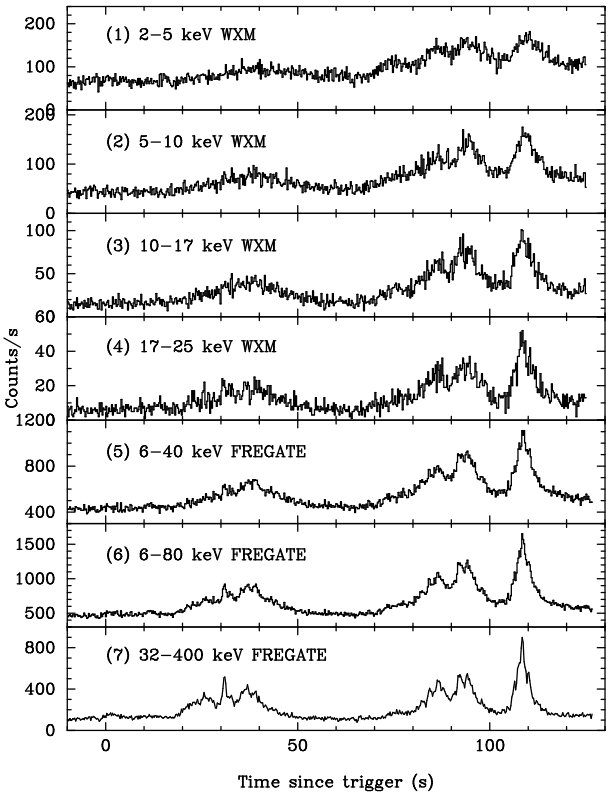

Fig. 2. Time history of GRB 020813 as observed by the *HETE*-2: WXM data (1) 2−5 keV, (2) 5−10 keV, (3) 10−17 keV, and (4) 17−25 keV bands; and FREGATE data (5) 6−40 keV, (6) 40−80 keV, and (7) 32−400 keV bands.

Moreover, the timescale of the temporal structure seems to be shorter at higher energies, which is a feature commonly observed in many GRBs (e.g., Fishman et al. 1992, Link et al. 1993, Fenimore et al. 1995). We can see a number of "shots" in the 32−400 keV light curve.

2.3. Spectrum

Two types of data sets ("*burst* data" and "*continuous* data") are provided by the FREGATE detector on board HETE-2 (Atteia et al. 2003). The burst data are only available when FREGATE triggered on the GRB, whereas continuous, monitoring data are always recorded whenever HETE-2 is operating. In a spectral analysis of FREGATE data, we usually use burst data, since it provides time- and energy-tagged photons with a much finer time resolution (6.4 μs) than the continuous data, which is accumulated every 5 s. However, due to the long duration of GRB 020813, the memory was full and burst data were only available at $0 \leq t \leq 70$ s. Therefore, we constructed the energy spectrum for the remaining part of the GRB by using continuous data over the full energy range of FREGATE (7−400 keV), which was also discrete data and only available during three separate intervals: $-120 \leq t \leq -40$ s, $40 \leq t \leq 120$ s, and $220 \leq t \leq 300$ s (figure 3, left). Note that the differences between the *burst* data and the *continuous* data are its time resolution and energy resolution. The quality of the

Table 1. Quoted errors corresponding to $\pm 1\sigma$.

Instrument	Energy (keV)	t_{90} (s)	t_{50} (s)
HETE-2 WXM	2−25	121.6 ± 1.2	34.4 ± 0.1
	2−5	129.0 ± 1.2	38.1 ± 1.3
	5−10	119.1 ± 2.2	33.2 ± 1.2
	10−25	99.5 ± 1.8	34.4 ± 1.7
HETE-2 FREGATE	6−400	87.9 ± 1.1	65.5 ± 0.8
	6−40	85.9 ± 0.3	32.7 ± 0.4
	40−80	89.0 ± 0.3	66.1 ± 0.7
	32−400	88.7 ± 0.6	67.3 ± 1.0

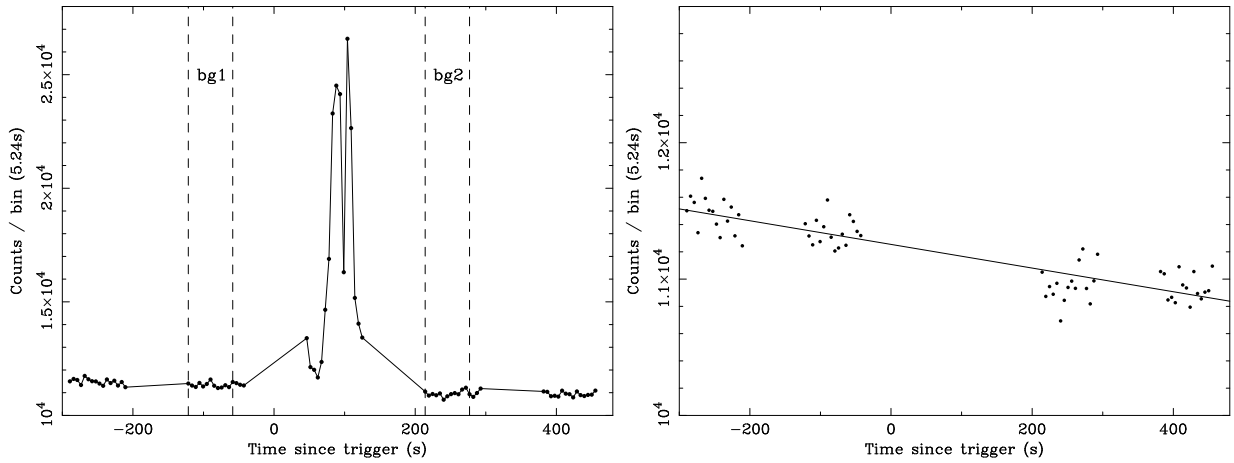

Fig. 3. *Left* : Light curve of the *continuous* data in the FREGATE energy band. *Right* : Background of the *continuous* data with a linear function.

derived spectra is exactly the same for both types of data in the following analysis.

The background level at an arbitrary time was estimated by interpolating the *pre*-burst *continuous* data ($-120 \leq t \leq -40$ s; bg1) and the *post*-burst *continuous* data ($220 \leq t \leq 300$ s; bg2) with a linear function of BG count $= 1.13 \times 10^4 - 0.87 \times t$, where t is the time after the burst in seconds (figure 3, *right*). We then calculated a weighted mean of the bg1 and the bg2 spectra at each time t, and subtracted this from the FREGATE spectral data.

To analyze the WXM data, we used the "TAG data" generated at the burst trigger time in the full 2−25 keV energy range. The background was integrated over 110 s, which was extracted from 118 s to 8 s before a burst. In the WXM spectral analysis, we considered only those events that registered on wires in the X- and the Y-detectors illuminated by the burst. Furthermore, since the variation in the gain is not uniform at the ends of the wires in the WXM detectors (Shirasaki et al. 2003), we used only the photon counts that registered in the central

±50 mm region of the wires to construct reliable spectra of the burst.

As one can see in figure 2, the light curve of GRB 020813 shows a very complex structure, such that four distinct peaks, at least, are visible in the light curve. Considering the fast time variability, we analyzed the spectrum of GRB 020813 every 5 s, which is also the limit imposed by the time resolution of the FREGATE continuous data.

Before going into the detailed spectral analysis, we first review the spectral evolution during a burst, by comparing the photon counting rates in the low energy (WXM) band with those in the high energy (FREGATE) bands. The hardness ratio of the fluxes, $S_\gamma(30-400$ keV) to $S_{\rm X}(2-30$ keV), is shown in figure 4 (third panel). One can see that GRB 020813 possibly consists of two distinct bursts that may have different physical origins. The border between the first and second bursts is approximately given by $t \sim 60$ s. Note that this corresponds to the epoch when the first gradual burst decayed to the initial (background) level, and succeeding flares started to appear in the light curve (figure 2).

We therefore denote the former part as "P1" and the latter part of the flare as "P2", just for convenience. The time intervals for P1 and P2 correspond to 17−52 s and 67−109 s from the burst trigger time, respectively. Note that the peak of P1 shows larger values of $S_\gamma(30-400$ keV)/ $S_{\rm X}(2-30$ keV) than that of P2, meaning that energy spectra in the peak of P1 are harder than those of P2.

In a more detailed analysis, we considered three different models to reproduce the observed spectra: (1) a power-law function, (2) a cutoff power-law function and (3) a Band function (Band et al. 1993). We first fitted the data with a single power-law function, but this model did not represent the spectra well, except in low photon statistics regions. This is because the spectrum of GRB 020813 is not a simple power-law, but bends sharply at high energies, as is often reported in other GRBs (e.g., Band et al. 1993). On the other hand, both the cutoff power-law and the Band function provide improved fits for all regions. Due to the limited photon statistics, it is hard to say which model is a better representation of the GRB 020813 spectra for each 5 s segment. We thus fit the time-averaged spectrum with a cutoff power-law and the Band function, and compared their results. When the photon statistics are sufficiently high, the Band function gives a better fit with a reduced χ^2 of 1.18 for 140 dof, compared to 1.33 for 141 dof for the cutoff power-law model. In the following analysis, we therefore use the Band function to discuss the evolution of the spectra for all time intervals.

Table 2 presents the results of a time-resolved spectral analysis of GRB 020813. We used the XSPEC version 11.2.0 software package to do the spectral fits. The photoelectric absorption in the direction of GRB 020813 is 7.0×10^{20} cm^{-2} (Vanderspek et al. 2002), which is negligible even in the WXM energy range above 2 keV. Therefore, we do not consider $N_{\rm H}$ as a parameter in the spectral analysis. Figure 4 summarizes the time evolution of spectral parameters together with the WXM and the FREGATE light curves measured at 2−25 keV and 7−400 keV, respectively (the first and the second panels). The time variations of the low

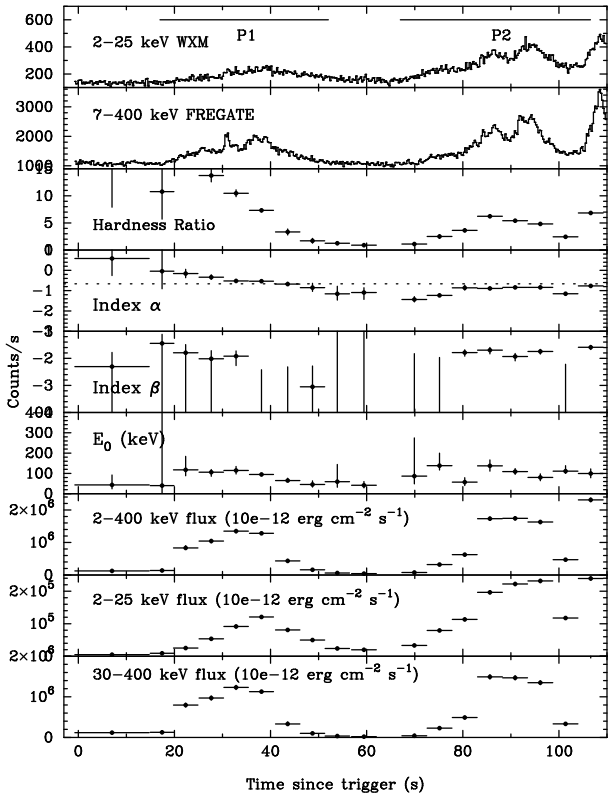

Fig. 4. Light curve and time evolution of the Band function parameters.

and high-energy photon indices, α and β, are plotted in the fourth and fifth panels. The break energy in the spectrum E_0 is given in the sixth panel, and the fluxes measured in the 2−400, 2−25 and 30−400 keV energy bands are plotted in the remaining panels.

As shown in figure 4, GRB 020813 spectra have a clear break around 100 keV, meaning that most of the power is emitted in the hard X-ray and the soft gamma-ray energy bands. For the time-averaged spectrum of P1, we found that $S_{\rm X}(2-30\ {\rm keV}) = (2.80 \pm 0.06) \times 10^{-6}$ ergs cm^{-2} and $S_\gamma(30-400\ {\rm keV}) = (2.53 \pm 0.07) \times 10^{-5}$ ergs cm^{-2}. Thus, the logarithmic fluence ratio, defined as $\log(S_{\rm X}/S_\gamma)$, is -0.96. Similarly, we obtain $\log(S_{\rm X}/S_\gamma) = -0.69$ for P2, with $S_{\rm X}(2-30\ {\rm keV}) = (8.20 \pm 0.14) \times 10^{-6}$ ergs cm^{-2} and $S_\gamma(30-400\ {\rm keV}) = (3.99 \pm 0.07) \times 10^{-5}$ ergs cm^{-2}. These results confirm that GRB 020813 belongs to the class of long classical GRBs according to the HETE classification method (Sakamoto et al. 2005).

However, we note that $\log(S_{\rm X}/S_\gamma) = -0.96$ is quite large compared to other GRB populations (Sakamoto et al. 2005) and would be at the extreme end of the classical GRB population. This is also indicated by the unusually *depletion* of low-energy (below E_0) photons observed in P1. In fact, the low-energy power-law indices, α, range from -1.16 to 0.0, some of which are much larger than expected from the "death line" ($\alpha = -0.67$). We will thus consider the origin of this low-energy depletion in the next section.

Table 2. Spectral model parameters of the Band function fit to the time-resolved spectra of GRB 020813.

Time interval (s) mid-time (start–end)	Photon index α (E^{α})	Photon index β (E^{β})	Cutoff energy (E_0 keV)	Reduced χ^2 (dof)
7.0 (-0.7 – 14.8)	$0.6^{+1.3}_{-0.8}$	$-2.3^{+0.5}_{-7.7}$	44^{+49}_{-20}	1.0 (18)
17.4 (14.9 – 19.9)	$-0.0^{+5.0}_{-1.0}$	$-1.5^{+0.4}_{-8.6}$	40^{+828}_{-37}	1.2 (27)
22.4 (19.9 – 24.9)	$-0.2^{+0.2}_{-0.2}$	$-1.8^{+0.3}_{-8.2}$	118^{+62}_{-30}	1.1 (35)
27.7 (25.1 – 30.2)	$-0.3^{+0.1}_{-0.1}$	$-2.0^{+0.3}_{-8.0}$	106^{+13}_{-21}	0.8 (47)
32.8 (30.2 – 35.4)	$-0.5^{+0.1}_{-0.1}$	$-1.9^{+0.2}_{-0.5}$	115^{+23}_{-20}	1.3 (57)
38.1 (35.5 – 40.7)	$-0.5^{+0.1}_{-0.1}$	$-9.4^{+6.8}_{-0.6}$	95^{+5}_{-9}	1.2 (58)
43.6 (41.0 – 46.2)	$-0.7^{+0.1}_{-0.1}$	$-9.4^{+7.2}_{-0.6}$	65^{+6}_{-5}	0.9 (45)
48.7 (46.2 – 51.3)	$-0.9^{+0.2}_{-0.2}$	$-3.1^{+0.8}_{-7.0}$	45^{+18}_{-13}	0.8 (29)
53.9 (51.3 – 56.5)	$-1.2^{+0.3}_{-0.3}$	$-9.4^{+19.4}_{-0.6}$	59^{+85}_{-31}	0.8 (30)
59.4 (56.8 – 62.0)	$-1.1^{+0.6}_{-0.3}$	$-9.4^{+19.4}_{-0.6}$	42^{+29}_{-28}	1.5 (30)
64.7 (62.0 – 67.3)*	—	—	—	—
69.9 (67.3 – 72.5)	$-1.4^{+0.1}_{-0.1}$	$-9.3^{+7.5}_{-0.7}$	87^{+188}_{-38}	0.8 (30)
75.2 (72.5 – 77.7)	$-1.2^{+0.1}_{-0.1}$	$-9.4^{+7.4}_{-0.6}$	138^{+62}_{-22}	0.8 (74)
80.4 (77.7 – 83.0)	$-0.9^{+0.1}_{-0.1}$	$-1.8^{+0.1}_{-0.1}$	57^{+22}_{-17}	1.0 (74)
85.7 (83.0 – 88.2)	$-0.9^{+0.1}_{-0.1}$	$-1.7^{+0.1}_{-0.2}$	138^{+33}_{-29}	1.2 (73)
90.9 (88.2 – 93.5)	$-0.8^{+0.1}_{-0.1}$	$-1.9^{+0.1}_{-0.2}$	109^{+15}_{-14}	1.2 (73)
96.1 (93.5 – 98.7)	$-0.8^{+0.1}_{-0.1}$	$-1.8^{+0.1}_{-0.1}$	80^{+18}_{-16}	0.8 (73)
101.4 (98.7 – 104.0)	$-1.2^{+0.1}_{-0.1}$	$-9.4^{+7.2}_{-0.6}$	111^{+27}_{-11}	0.9 (68)
106.6 (104.0 – 109.2)	$-0.8^{+0.1}_{-0.1}$	$-1.6^{+0.1}_{-0.1}$	100^{+26}_{-24}	1.3 (73)

* The spectral parameters cannot be determined for the time interval 62.0–67.3 due to poor statistics.

3. Discussion

3.1. Origin of Low-Energy Depletion in P1

As we have discussed in the previous section, GRB 020813 shows a depletion of low-energy photons, especially in the P1 region. Such flat spectra, exceeding the "death line" ($\alpha = -0.67$; Preece et al. 2000), have already been reported in a number of BATSE (Burst and Transient Source Experiment) GRBs, though they were not conclusive due to the limited sensitivity of BATSE at low energies. Frontera et al. 2000, using the BeppoSAX WFC and GRBM, reported that a few GRBs show significant low-energy depletion in 2–20 keV, though their energy coverages of WFC and GRBM are not completely continuous, and the energy resolution of GRBM was somewhat limited. Therefore, the HETE-2 observation of GRB 020813 presents an independent measurement of a similar characteristic spectra with higher reliability over the wide and continuous energy range (2–400 keV) of HETE-2. In the following, we

examine various scenarios to understand the origin of the X-ray emission from GRB 020813.

First, we consider the spectral hardening due to synchrotron self-absorption (SSA). We can define a critical frequency, $\nu_{\rm a}$, where the plasma becomes optical thick, resulting in a hard X-ray spectrum with $\alpha = +1$ well below $\nu_{\rm a}$ (e.g., Sari et al. 1998). Meanwhile, the high-energy spectral index of GRB 020813, $\beta \sim -2.15$, is that expected from a "fast cooling" of electrons with its power-law index, -2.3 ($= 2\beta{+}2$). Therefore, a sharp spectral break, as observed in GRB 020813, is expected only when the minimum synchrotron frequency, $\nu_{\rm m}$, is *degenerate* with respect to $\nu_{\rm a}$, such that $h\nu_{\rm m} \sim h\nu_{\rm a} \sim E_0$.

In this particular case, the observed SSA frequency is approximately given as [2]

$$\nu_{\rm a} \sim 14.5 \times (1+z)^{-1} (rn)^{3/5} B^{2/5} \sim 6.4 \times (rn)^{3/5} B^{2/5} \ \ {\rm Hz}, \tag{1}$$

where z is the redshift, r (cm) the radius of emission volume, n (cm^{-3}) the electron number density, and B (gauss) the magnetic field strength (Dermer et al. 2000). Then, the peak frequency of the synchrotron radiation in the observer's frame is given as

$$\nu_{\rm m} \sim 1.2 \times 10^6 (1+z)^{-1} B\delta\gamma_{\rm m}^2 \sim 5.3 \times 10^5 B\delta\gamma_{\rm m}^2 \ \ {\rm Hz} \tag{2}$$

(Rybicki, Lightman 1979). Combining equations (1) and (2) to eliminate B, and normalizing to typical values for GRBs, the electron number density is given by

$$n = 3.0 \times 10^{15} \left(\frac{r}{10^{10}}\right)^{-1} \left(\frac{\nu_{\rm a}}{10^{19}}\right)^{5/3} \left(\frac{\nu_{\rm m}}{10^{19}}\right)^{-2/3} \left(\frac{\gamma_{\rm m}}{100}\right)^{2} \ \ {\rm cm}^{-3}. \tag{3}$$

In figure 5, we plot the allowed parameter space for the region size r and the electron number density n of GRB 020813. Here, we have assumed $\nu_{\rm a} = \nu_{\rm m} = 10^{19}$ Hz. Equation (3) is represented by line (I).

Then, from the electron energy density, $u_{\rm e} \simeq n\gamma_{\rm m} m_{\rm e} c^2$, and the magnetic field energy density, $u_{\rm B} = B^2/8\pi$, with $u_{\rm e} \equiv \xi u_{\rm B}$, we obtain

$$n = 1.7 \times 10^{17} \xi \left(\frac{\nu_{\rm m}}{10^{19}}\right)^{2} \left(\frac{\gamma_{\rm m}}{100}\right)^{-7} \ \ {\rm cm}^{-3}. \tag{4}$$

Equations for the cases of $\xi = 0.1$, 1, and 10 are represented by lines (II) in figure 5.

Finally, from the relation $\frac{4}{3}\pi r^3 u_{\rm e} = \epsilon_{\rm e} E_{\rm tot}$, we obtain

$$n = 2.9 \times 10^{24} \left(\frac{r}{10^{10}}\right)^{-3} \left(\frac{\gamma_{\rm m}}{100}\right)^{-1} \left(\frac{\epsilon_e}{0.1}\right) \left(\frac{E_{\rm tot}}{10^{52}}\right) \ \ {\rm cm}^{-3}, \tag{5}$$

where $\epsilon_{\rm e}$ is the fraction of the shock energy given to the electrons and $E_{\rm tot}$ is the total explosion energy of GRB 020813, 1.2×10^{53} ergs (2$-$400 keV), calculated from the observed fluence and duration of P1. Equations for the cases of $\epsilon_{\rm e} = 0.001$, 0.1, and 0.5 are represented by lines (III) in figure 5.

[2] Using an approximate relation of $\delta \sim \Gamma_{\rm BLK} \sim \gamma_{\rm m}$, where δ is the Doppler beaming factor, $\gamma_{\rm m}$ is the minimum electron Lorentz factor and $\Gamma_{\rm BLK}$ is the bulk Lorentz factor. Assuming a viewing angle between the GRB and observer $\theta \sim \frac{1}{\Gamma_{\rm BLK}}$, we can derive $\delta \sim \Gamma_{\rm BLK}$. Furthermore, we assume $\gamma_{\rm m}/\Gamma_{\rm BLK}$ [see, equation (1)] is of order unity as often assumed in modeling the GRB emission.

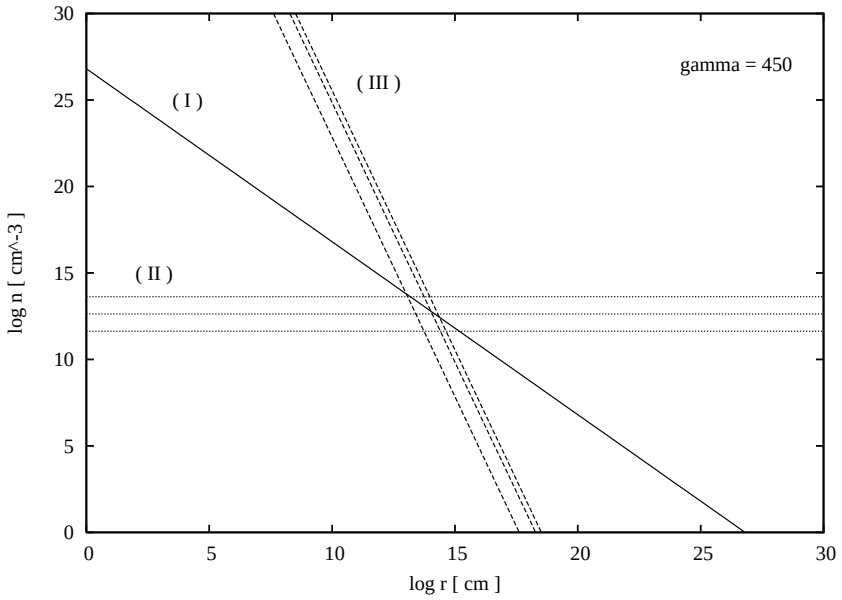

Fig. 5. Parameter space (n, r) allowed by the SSA model with $\nu_{\rm a} = \nu_{\rm m}$ of 10^{19} Hz and $E_{\rm tot}$ of 1.2×10^{53} ergs. Line (I) was derived from the SSA frequency. Lines (II) were derived from relation of the energy density of the electrons and the magnetic field. Here, we used $\xi = 0.1$, 1, and 10 (from bottom to top). Lines (III) were derived from a calculation of the total energy of the electrons. Here, we used $\epsilon_e = 0.001$, 0.1, and 0.5 (from left to right). The crossing point of the three expressions indicated the allowed parameters for the SSA model.

As can be seen in figure 5, the most likely parameters for the SSA model would be a region defined by the crossing of three different lines. These are $n \sim 4.5 \times 10^{12}$ cm^{-3}, $r \sim 1.4 \times 10^{14}$ cm, $\gamma_{\rm m} \sim 450$, and $B \sim 2.1 \times 10^5$ gauss, assuming $\xi = 1$ and $\epsilon_{\rm e} \sim 0.1$.

Using these parameters, the peak flux is $\sim 10^9$ ergs cm^{-2} s^{-1}, calculated from $\nu F(\nu) = \frac{\nu}{4\pi d_{\rm L}^2} \int d^3\vec{r} [4\pi j_\nu(\vec{r}) exp(-\int \alpha_\nu(\vec{r'} ds'))]$, where j_ν is the synchrotron emission coefficient and α_ν is the self-absorption coefficient (e.g., Rybicki, Lightman 1979). It is more than 15 orders of magnitude different from the observed value, 10^{-6} ergs cm^{-2} s^{-1}. In other words, in order to observe $\nu_{\rm a}$ in the hard X-ray band, we have to choose unusual parameters, such as $\epsilon_e \ll 10^{-10}$, in contrast to the standard GRB fireball model (e.g., Piran 1999).

As another possible scenario, we consider the special case that the hard X-ray spectrum is the low-energy end of the inverse Compton emission, which could be a "mirror" of the synchrotron self-absorption spectrum in the radio band (e.g. Liang et al. 1997). For this case, the synchrotron emission spectrum is boosted by a factor of $\gamma_{\rm m}^2$ via inverse Compton scattering of synchrotron photons. Therefore, we assume $\gamma^2 \nu_{\rm a} \equiv \nu_{\rm c,a} \sim 10^{19}$ Hz and $\gamma^2 \nu_{\rm m} \equiv \nu_{\rm c,m} \sim 10^{19}$ Hz.

In figure 6, we show the allowed values of n as a function of r for the Synchrotron self-Compton (SSC) model. As in figure 5, we found parameters of the allowed region: $n = 4.6 \times 10^4$ cm^{-3}, $r = 6.5 \times 10^{16}$ cm, $\gamma_{\rm m} \sim 260$, and $B = 16$ gauss, assuming $\xi = 1$ and $\epsilon_{\rm e} \sim 0.1$. Note that a 10^{16} cm radius is close to the typical value of the "afterglow" emission, rather than the prompt

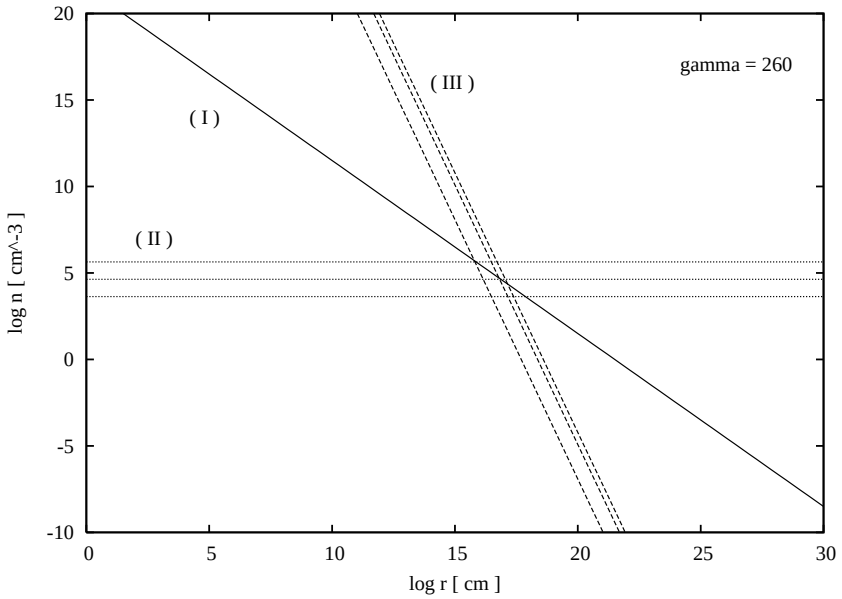

Fig. 6. Parameter space (n, r) allowed by the SSC model with $\nu_{\rm c,a}$ of 10^{19} Hz, $\nu_{\rm c,m}$ of 10^{19} Hz, and $E_{\rm total}$ of 5.8×10^{51} ergs. Lines (I), (II), and (III) represent the same relations as in figure 5. The crossing point of the three expressions indicates the allowed parameters for the SSC model.

GRB emission (e.g., Piran 1999). We therefore conclude that the SSC model for the hard X-ray spectrum is also unlikely in the standard fireball scenario.

Thus, it is difficult to explain the P1 spectrum of GRB 020813 by either the SSA or SSC model. Therefore, we consider other radiation processes, such as "jitter" radiation and Compton drag effects. Medvedev (2000) pointed out that the radiation emitted by ultra-relativistic electrons in highly nonuniform, small-scale magnetic fields is different from synchrotron radiation if the electron's transverse deflections in these fields are much smaller than the beaming angle. He showed that the spectral power distribution of the radiation produced by the power-law distributed electrons is well described by a sharply broken power-law, $\propto \nu^1$ for $\nu \leq \nu_{\rm jb}$ and $\propto \nu^{-(p-1)/2}$ for $\nu \geq \nu_{\rm jb}$, where p is the electron power-law index and $\nu_{\rm jb}$ is the jitter break frequency (Medvedev 2000).

Therefore, the low-energy depletion (α is larger than the death-line) with a spectral break may be naturally explained by jitter radiation. In this model, the spectral break due to jitter will be observed at

$$\nu_{\rm m} \sim 6.0 \times 10^{15} \left(\frac{\gamma_{\rm m}}{100}\right)^3 \left(\frac{\gamma_{\rm int}}{1}\right) \left(\frac{\gamma_{\rm e}}{1}\right)^{-1/2} \left(\frac{n}{10^{10}}\right)^{1/2} \ {\rm Hz}, \tag{6}$$

where $\gamma_{\rm int}$ is the relative Lorentz factor of two colliding shells, $\gamma_{\rm int} \sim 2-4$, and $\gamma_{\rm e}$ is the initial effective thermal Lorentz factor, $\gamma_{\rm e} \sim 2-3$ (Medvedev 2000). If $\gamma_{\rm m}$ is close to 1000, $\nu_{\rm m}$ can be observed in the X-ray band. In the realistic case, the emergent spectrum is determined by the statistical properties of the magnetic field in the emission region. If the magnetic field is highly inhomogeneous, jitter radiation may overcome the synchrotron radiation, whereas the reverse

applies for the uniform magnetic field cases. Therefore, it is possible that the X-ray spectrum of GRB 020813 (P1 region) may be a mixture of jitter radiation with the usual synchrotron radiation component, but detailed modeling of the spectrum is beyond the scope of this paper.

As an alternative idea, Lazzati et al. (1999) and Ghisellini et al. (2000) proposed that the gamma-ray photons that characterize the prompt emission of GRBs are produced through the Compton drag process, caused by the interaction of a relativistic fireball with a very dense soft photon bath. This is an interesting assumption, because some of the GRBs are indeed associated with supernovae, where the expanding star can provide enough soft photons to make the radiative drag effective.

This model accounts for the basic properties of GRBs, i.e., the overall energetics and the peak frequency of the spectrum, with a radiative efficiency of more than 50%. Also note that the GRB should have a very hard spectrum $\propto \nu^2$, as expected from the Rayleigh-Jeans law below the peak frequency of the emission. In fact, our spectral shape is in good agreement with the spectra produced by Compton drag for $\Gamma_0 = 300$ (Ghisellini et al. 2000). The major weakness of this model is that the predicted spectrum is basically thermal, and a typical power-law spectrum is not always produced. Thus, we find that both the jitter radiation and the Compton drag may reproduce the low-energy depletion observed in GRB 020813.

However, we note that a complete theoretical interpretation of the data is beyond the scope of this paper. There are other theoretical models that can explain the spectra with low-energy depletion.

3.2. Spectrum in P2

The average P2 spectrum is well described by the Band function with $\alpha \sim -1.00$ and $\beta \sim -1.76$. In contrast to P1, α falls in the range allowed by the standard synchrotron shock model (SSM). As shown by Sakamoto et al. (2005), integration of the BATSE and the HETE-2 data revealed that the "typical" GRB spectrum is well represented by a broken power-law (Band) function with $\alpha \sim -1$ and $\beta \sim -2.5$. Therefore, the observed break energy corresponds to the peak energy ($\nu \sim \nu_{\rm m}$) in $\nu {\rm F}_\nu$ space, which is where most of the GRB power is emitted. For the case of P2 in GRB 020813, however, the spectrum is still *rising* up to > 400 keV. [3] In the standard picture of SSM, such a break could be explained only when $\nu_{\rm m}$ is well above the HETE bandpass, which again seems to be quite different from the P1 spectrum.

We stress, however, that it does not seem to be strange even if P1 and P2 show quite different spectral features, since they constitute distinct "peaks" both in the light curve and in the hardness ratio (figure 4). According to the internal shock scenario (e.g., Piran 1999), GRB light curves are thought to be produced by the collisions of shells that are moving with different Lorentz factors. A fraction of the bulk kinetic energy is converted to the random energy of

[3] Since the detection limit of HETE-2 is 400 keV, it is difficult to discuss the slope of the high-energy power-law above 400 keV. It is necessary to consider the results from a higher energy detector such as Konus.

electrons, which emit the *observed* radiation as prompt GRB emission. Since the radiation from each two-shell collision would be observed as a single pulse, P1 and P2 may be attributed to the collisions of different pairs of shells, which are possibly taking place in different physical conditions (e.g., magnetic field, density of material).

A detailed simulation of a collisionless shock plasma predicts that the magnetic field produced in GRB shocks randomly fluctuates on a very small scale of the relativistic skin depth, which is $\lambda \sim 10^2$ cm in internal shocks (Medvedev, Loeb 1999). Meanwhile, the emitting ultrarelativisitic electrons have much larger Larmor radii. In such situations, jitter radiation may overcome the usual synchrotron radiation, but it is also likely that the large scale fields are also present in the GRB ejecta. Therefore, the dominance of the "synchrotron" and the "jitter" radiation would be determined by a combination of large-scale fields ($B_{\rm LS}$) and non-uniform, small-scale magnetic fields ($B_{\rm SS}$). We mention in this context that the different observed properties in P1 and P2 may reflect the different balance of large/small-scale magnetic fields, where $B_{\rm SS} \geq B_{\rm LS}$ for P1 and $B_{\rm SS} \geq B_{\rm LS}$ for P1 and $B_{\rm SS} \leq B_{\rm LS}$ for P2, but further study using more data is necessary to confirm this.

4. Conclusion

In this paper we reported HETE-2 WXM/FREGATE observations of bright and long GRB 020813. Our observational results demonstrate that the peak P1 (17−52 s) of the burst shows a depletion of low-energy photons below about 50 keV. Therefore, we examined various scenarios to understand the origin of such a low-energy depletion. We conclude that it is difficult to explain the depletion by either the SSA or SSC model. One possibility is that the low-energy depletion may be understood as a mixture of "jitter" radiation with the usual synchrotron radiation component. On the other hand, the spectrum of P2 (67−109 s) can be explained by the standard SSM. We believe that the magnetic field is uniform and that synchrotron radiation may overcome the jitter radiation in this region.

We are grateful to R. Yamazaki for giving useful advise concerning our discussions. The HETE-2 mission is supported in the US by NASA contract NASW-4690; in Japan in part by Grant-in-Aid (14079102 and 14GS0211) from the Ministry of Education, Culture, Sports, Science, and Technology; and in France by CNES contract 793-01-8479. K.H. is grateful for support under MIT-SC-R-293291.

References

Atteia, J.-L., et al. 2003, in Gamma-Ray Burst and Afterglow Astronomy 2001, ed. G. R. Ricker & R. K. Vanderspek (New York:AIP), 17

Band, D., et al. 1993, ApJ, 413, 281

Barth, A. J., et al. 2003, ApJ, 584, L47

Covino, S., et al. 2003, A&A 404, L5
Dermer, C. D., Böttcher, M., & Chiang, J. 2000, ApJ, 537, 255
Fishman, G. J., Meegan, C. A., Wilson, R. B., Horack, J. M., Brock, M. N., Paciesas, W. S., Pendleton, G. N., & Kouveliotou, C. 1992, in Gamma-Ray Bursts: Huntsville, 1991, ed. W. S. Paciesas & G. J. Fishman (New York: AIP), 13
Fenimore, E. E., in 't Zand, J. J. M., Norris, J. P., Bonnell, J. T., & Nemiroff, R. J. 1995, ApJ, 448, L101
Fox, D. W., Blake, C., & Price, P. 2002, GRB Coord. Netw. Circ., 1470
Frontera, F., et al. 2000, ApJS, 127, 59
Ghisellini, G., Lazzati, D., Celotti, A., & Rees, M. J. 2000, MNRAS, 316, 45
Hurley, K., et al. 2002a, GRB Coord. Netw. Circ., 1482
Hurley, K., et al. 2002b, GRB Coord. Netw. Circ., 1483
Lazzati, D., Ghisellini, G., Celotti, A., & Rees, M. J. 2000, ApJ, 529, L17
Liang, E., Kusunose, M., Smith, I. A., & Crider, A. 1997, ApJ, 479, L35
Link, B., Epstein, R. I., & Priedhorsky, W. C. 1993, ApJ, 408, L81
Medvedev, M. V. 2000, ApJ, 540, 704
Medvedev, M. V., & Loeb, A. 1999, ApJ, 526, 697
Piran, T. 1999, Phys. Rep., 314, 575
Preece, R. D., Briggs, M. S, Mallozzi, R. S., & Pendleton, G. N. 1998, ApJ, 506, L23
Preece, R. D., Briggs, M. S, Mallozzi, R. S., Pendleton, G. N., Paciesas, W. S., & Band, D. L. 2000, ApJS, 126, 19
Rybicki, G. B. & Lightman, A. P. 1979, Radiative Processes in Astrophysics (New York: Wiley-Interscience)
Sakamoto, T., et al. 2005, ApJ, 629, 311
Sari, R., Piran, T., & Narayan, R. 1998, ApJ, 497, L17
Shirasaki, Y., et al. 2003, PASJ, 55, 1033
Tavani, M. 1996, ApJ, 466, 768
Urata, Y., et al. 2003, ApJ, 595, L21
Vanderspek, R., Marshall, H. L., Ford, P. G., & Ricker, G. R. 2002, GRB Coord. Netw. Circ., 1504